Electronics and Electrical Engineering

AIMS Electronics and Electrical Engineering, 8(3): 370–393.
DOI: 10.3934/electreng.2024018
Received: 08 July 2024
Revised: 12 August 2024
Accepted: 02 September 2024
Published: 06 September 2024

https://www.aimspress.com/journal/ElectrEng

Research article

Combining fractional-order PI controller with field-oriented control based on maximum torque per ampere technique considering iron loss of induction motor

Fadhil A. Hasan*and Lina J. Rashad

Department of Electrical Engineering, University of Technology, Iraq

*** Correspondence:** E-mail: fadhil.a.hasan@uotechnology.edu.iq; Tel: +964-780-156-3135.

Abstract: This paper presents a combined approach of fractional-order proportional-integral (FOPI) control with field-oriented control (FOC) for maximum torque per ampere (MTPA) tracking. The method maximizes the torque-to-ampere ratio by optimizing the produced torque and minimizing the stator current. This approach reduces power consumption and thereby enhances energy efficiency. Furthermore, the method is improved by considering the rotor iron loss (closest to reality). The complete mathematical analysis, modeling, and simulation are demonstrated. The dominant criteria of the motor, such as rotor speed, electromagnetic torque, and stator current, were compared with the conventional FOC technique. Results showed that the proposed approach significantly exceeds the conventional FOC in terms of drawing current and power consumption, with a 31%–47% and 35%–40% reduction in stator current and average starting current, respectively. Besides, the torque/ampere ratio increased by an average of 24%–39%, with a 12%–17% decrease in consumed kWh for a specific period. The only drawback of the proposed method is that it slightly degrades speed performance, which can simply be ignored. These findings validate the effectiveness of the proposed strategy, especially for battery-powered applications such as electric vehicles.

Keywords: maximum torque per ampere; fractional order PI controller; field-oriented control; energy efficiency; induction motor control

List of nomenclature

Nomenclature	Description
Superscripts: s, e	Stationary and rotating reference frames
Subscripts: s, r, m, l	Stator, rotor, and magnetizing circuits, leakage flux
Subscripts: d, q	Direct and quadrature axis
v, i, ψ	Voltage, current, flux vectors
r, x	Resistance and reactance
$\omega_e, \omega_r, \omega_s$, ω_b	Synchronous, rotor, slip, and based speeds
$\mathcal{F}^e_{ds}, \mathcal{F}^e_{qs}$	Direct and quadrature stator magnetic fields
$\mathcal{F}^e_{dr}, \mathcal{F}^e_{qr}$	Direct and quadrature rotor magnetic fields
$\mathcal{F}^e_{dm}, \mathcal{F}^e_{qm}$	Direct and quadrature magnetizing fields
L_{ls}, L_{lr}	Stator and rotor leakage inductances
L_M	Magnetizing inductance
P	Number of poles
T_e, T_L	Electromagnetic and load torques
J	Moment of inertia
R_w	Iron loss equivalent resistance
${}_{t_o}^{C}\mathcal{D}_t^{\beta}$	Caputo's differ-integral operator
β	Caputo's fractional order
k_P, k_I, k_D	Proportional, integral, and derivative gains
λ,	Integral and derivative fractional orders

List of abbreviations

Abbreviation	Description
FOPI	Fractional order proportional integral
FOC	Field-oriented control
MTPA	Maximum torque per ampere
PI	Proportional integral
IM	Induction motor
DTC	Direct torque control
MRAS	Model reference adaptive system
ST-SMO	Super-twisting sliding mode observer
MPCC	Model predictive current control
FLC	Feedback linearization control
EV	Electric vehicle
IOFL	Input-output feedback linearization
ANN	Artificial neural network
PSO	Particle swarm optimization

1. Introduction

The three-phase induction motor (IM) is essential in various electric applications and is integral in operating machines, pumps, fans, compressors, and others, due to its robustness, reliability, and low cost. The power consumed by electrical motors is about 42%–48% of total international electricity consumption [1]. Thus, it is essential to improve the efficiency of motor drives. Significant power saving can be achieved by even slightly enhancing energy efficiency. The amount of starting, dynamic, and steady-state currents in motor drives is essential to increasing efficiency. Several traditional controlling methods exist in the literature for induction motors, such as scalar controllers, vector or field-oriented control (FOC), and direct torque control (DTC) [2]. While these controllers have been effective in dynamic and steady-state performance, they often face the challenges and drawbacks of high current consumption under various load conditions. This relates to the fact that if high-speed torque performance is required, then high input power is required. These limitations emphasize the need for more advanced control techniques to improve motor drive efficiency and reduce loss [3].

Maximum torque per ampere (MTPA) tracking is an efficient technique in motor drives, aiming to optimize torque production while minimizing current consumption. This approach is important for enhancing motor efficiency, reducing losses, and achieving optimal motor performance, especially in applications where energy efficiency has priority, such as electric vehicles [2,3]. The fractional-order proportional-integral (FOPI) controller has earned the attention of researchers because of its ability to enhance control accuracy and robustness compared to traditional integer-order PI controllers. Thus, FOPI controllers became a favorable choice for improving dynamic response, disturbance rejection, and system stability [4].

Various efforts have been made to enhance and optimize motor performance. V. Kousalya and Bhim Singh (2023) presented an optimized operating point (OOP) to reduce power consumption and enhance the induction motor's efficiency. The authors combined the model reference adaptive system (MRAS) with a super-twisting sliding mode observer (ST-SMO). The results showed significantly reduced consumed power and enhanced efficiency [5]. Qifeng Ding et al. (2023) proposed a bearing-less IM with specific poles to enhance efficiency. An optimal rotor field-oriented control strategy was presented. The results showed improved motor efficiency and excellent levitation performance [6]. Mateo Bašić et al. (2023) presented model predictive current control (MPCC) for complex modeling of induction motors, including magnetic saturation and loss. The control effort penalization strategy was used to reduce the losses of the power converter. The results showed improved performance compared to conventional field-oriented control drives [7]. Tomáš Lažek et al. (2022) compared two loss minimization algorithms for IM drives based on the Gamma and inverse Gamma networks. The algorithms aimed to find the optimal flux that minimizes losses at the desired torque and speed. The results showed an enhancement in efficiency with more reduced derivation complexity [8]. Kousalya V. et al. (2022) introduced a loss reduction model–based maximum torque per ampere control for IM. The loss model considers iron loss and magnetic saturation. The model was simplified as a dependent voltage source in series with iron loss resistance. The MTPA strategy optimized flux reference while considering stator current reduction. Simulations demonstrated a decrease in power consumption and improved efficiency [9]. Angelo Accetta et al. (2022) introduced a feedback linearization control (FLC) technique for linear induction motors, considering the dynamic iron loss. Various air-gap field values enhanced the FOC and FLC performances [10]. C.

Attaianese et al. (2021) presented the FOC technique with the maximum torque per watt technique to minimize the loss in the stator and rotor circuits. The results demonstrated significant improvements in the efficiency of the IM drives [11]. S. Rasul Eftekhari et al. (2020) presented a robust predictive torque control of induction motors based on the loss model. The results showed a fast dynamic response with minimizing motor losses [12]. Hafiz Muhammad et al. (2019) enhanced the performance of the electric vehicle (EV) traction system using the nonlinear FOPI controller. A Li-ion battery was used to drive the induction motor in a prototype EV model. The results verified that the proposed method was robust and efficient for EV traction [13]. In Mohammad-Ali Salahmanesh et al. (2019), the nonlinear field-oriented control was presented using the input-output feedback linearization (IOFL) method. Besides, the model-based maximum torque per ampere control was presented. Simulation results demonstrated the effectiveness of the proposed controller [14]. Adil Khurram et al. (2018) investigated the performance of the fractional-order PI controller compared to the linear PI controllers. The FOPI controller was designed using various tuning methods of the PI controller. The results indicated that the FOPI controller showed better dynamic performance in conjunction with traditional methods [15]. G. Madhusudhana Rao and G. Srikanth (2018) introduced a novel maximum torque per ampere controller for induction motor drives that employs an output artificial neural network (ANN)-based feedback linearization to design a torque- and flux-compensating model. The results showed optimized MTPA and improved efficiency of electromechanical energy conversion [16].

Among those works, it has not yet been attempted to combine the FOPI-FOC and MTPA. For the first time, this paper proposes the optimum FOPI-FOC-MTPA controller to maximize the torque-per-ampere ratio with adequate speed performance. The significant contribution of integrating FOPI-FOC-MTPA in induction motors is evident in many enhancements such as robustness, efficiency, performance, reliability, and adaptability. Besides, it reduces energy consumption and operating costs, which makes it environmentally sustainable and economically beneficial. Minimizing current flow while maximizing torque production reduces motor heating and mechanical stress. These valuable advancements in motor control technology have diverse applications in various industries. The FOPI-FO controller is optimized using particle swarm optimization (PSO) intelligence in offline mode, which was adopted in this work. This approach increases the robustness and nonlinearity ability of the drive system.

2. Induction motor mathematical model

The synchronously rotating reference frame model of the IM is preferred in dynamic analysis. The electrical variables in the model can be expressed as voltage, current, and flux. The state-space equations of the machine in a rotating frame with flux linkages as the primary variables will derive the IM model. The superscript (e) refers to the rotating reference frame. Assuming all rotor parameters are referred to the stator circuit, the rotor winding is short-circuited, and the input variable is the stator currents. The direct and quadrature equivalent circuits of the induction motor (in a rotating reference frame) are shown in Figure 1.

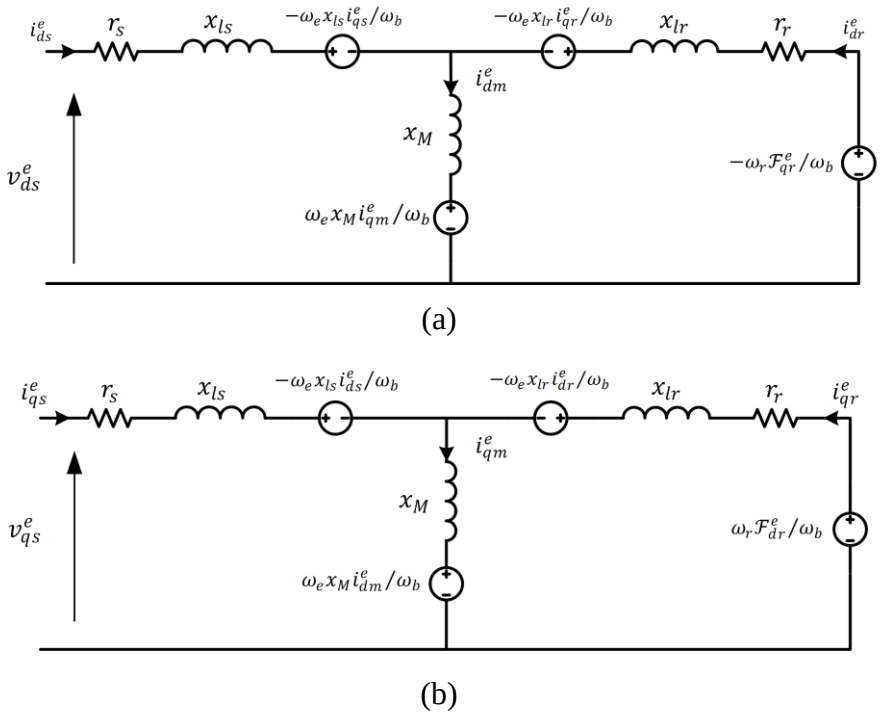

Figure 1. Rotating reference frame equivalent circuits, (a) d-axis, (b) q-axis.

The state space equations can be derived as follows [17–19]:

$$v^e_{qs} = r_s i^e_{qs} + \dot{\mathcal{F}}^e_{qs}/\omega_b + \omega_e \mathcal{F}^e_{ds}/\omega_b \tag{1}$$

$$v^e_{ds} = r_s i^e_{ds} + \dot{\mathcal{F}}^e_{ds}/\omega_b - \omega_e \mathcal{F}^e_{qs}/\omega_b \tag{2}$$

$$0 = r_r i^e_{qr} + \dot{\mathcal{F}}^e_{qr}/\omega_b + (\omega_e - \omega_r)\mathcal{F}^e_{dr}/\omega_b \tag{3}$$

$$0 = r_r i^e_{dr} + \dot{\mathcal{F}}^e_{dr}/\omega_b - (\omega_e - \omega_r)\mathcal{F}^e_{qr}/\omega_b \tag{4}$$

Where,

$$\mathcal{F}^e_{qs} = \omega_b \psi_{qs} = x_{ls} i^e_{qs} + x_M (i^e_{qs} + i^e_{qr}) \tag{5}$$

$$\mathcal{F}^e_{ds} = \omega_b \psi_{ds} = x_{ls} i^e_{ds} + x_M (i^e_{ds} + i^e_{dr}) \tag{6}$$

$$\mathcal{F}^e_{qr} = \omega_b \psi_{qr} = x_{lr} i^e_{qr} + x_M (i^e_{qs} + i^e_{qr}) \tag{7}$$

$$\mathcal{F}^e_{dr} = \omega_b \psi_{dr} = x_{lr} i^e_{dr} + x_M (i^e_{ds} + i^e_{dr}) \tag{8}$$

$$\mathcal{F}^e_{qm} = \omega_b \psi_{qm} = x_M (i^e_{qs} + i^e_{qr}) \tag{9}$$

$$\mathcal{F}^e_{dm} = \omega_b \psi_{dm} = x_M (i^e_{ds} + i^e_{dr}) \tag{10}$$

Where,

$$x_{ls} = \omega_b L_{ls} \tag{11}$$

$$x_{lr} = \omega_b L_{lr} \tag{12}$$

$$x_M = \omega_b L_M \tag{13}$$

Then,

$$\mathcal{F}_{qs}^e = \omega_b \psi_{qs} = x_S i_{qs}^e + x_M i_{qr}^e \tag{14}$$

$$\mathcal{F}_{ds}^e = \omega_b \psi_{ds} = x_S i_{ds}^e + x_M i_{dr}^e \tag{15}$$

$$\mathcal{F}_{qr}^e = \omega_b \psi_{qr} = x_R i_{qr}^e + x_M i_{qs}^e \tag{16}$$

$$\mathcal{F}_{dr}^e = \omega_b \psi_{dr} = x_R i_{dr}^e + x_M i_{ds}^e \tag{17}$$

$$i_{qs}^e = \frac{\mathcal{F}_{qs}^e - x_M i_{qr}^e}{x_S} \tag{18}$$

$$i_{ds}^e = \frac{\mathcal{F}_{ds}^e - x_M i_{dr}^e}{x_S} \tag{19}$$

$$i_{qr}^e = \frac{\mathcal{F}_{qr}^e - x_M i_{qs}^e}{x_R} \tag{20}$$

$$i_{dr}^e = \frac{\mathcal{F}_{dr}^e - x_M i_{ds}^e}{x_R} \tag{21}$$

Then,

$$v_{qs}^e = r_s(\mathcal{F}_{qs}^e - x_M i_{qr}^e)/x_S + \dot{\mathcal{F}}_{qs}^e/\omega_b + \omega_e \mathcal{F}_{ds}^e/\omega_b \tag{22}$$

$$v_{ds}^e = r_s(\mathcal{F}_{ds}^e - x_M i_{dr}^e)/x_S + \dot{\mathcal{F}}_{ds}^e/\omega_b - \omega_e \mathcal{F}_{qs}^e/\omega_b \tag{23}$$

$$0 = r_r(\mathcal{F}_{qr}^e - x_M i_{qs}^e)/x_R + \dot{\mathcal{F}}_{qr}^e/\omega_b + \omega_s \mathcal{F}_{dr}^e/\omega_b \tag{24}$$

$$0 = r_r(\mathcal{F}_{dr}^e - x_M i_{ds}^e)/x_R + \dot{\mathcal{F}}_{dr}^e/\omega_b - \omega_s \mathcal{F}_{qr}^e/\omega_b \tag{25}$$

Where $\omega_s = \omega_e - \omega_r$

$$T_e = \frac{3P}{4\omega_b}(\mathcal{F}_{dr}^e i_{qr}^e - \mathcal{F}_{qr}^e i_{dr}^e) \tag{26}$$

3. FOC-combined MTPA technique

Field-oriented control demonstrates that the induction motor can be controlled like a separately excited DC motor, bringing a renaissance in the high-performance control of AC drives. Undoubtedly, FOC will oust scalar control and be accepted as the industry-standard control for AC drives [18]. The principal idea of this method is to decouple the inherent coupling between the torque and field

currents to ensure constant airgap flux during torque and speed control. This can easily be done by aligning the rotor flux vector along the d-axis of the rotating frame, as shown in Figure 2.

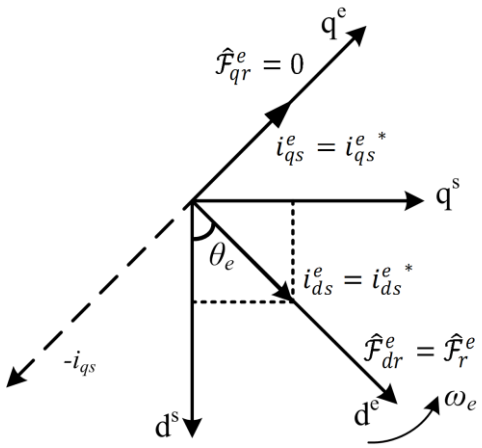

Figure 2. Vector diagram of correct field orientation.

This means that when $i_{qs}^{e\,*}$ is controlled, it affects the actual i_{qs}^{e} current only but does not affect the flux $\mathcal{F}_{\mathrm{r}}^{\mathrm{e}}$. Similarly, when $i_{ds}^{e\,*}$ is controlled, it controls the flux only (remains constant) and does not affect the i_{qs}^{e} component. Accordingly, the rotor flux components become [5, 18]:

$$\mathcal{F}_{qr}^{e} = 0 \implies \left|\hat{\mathcal{F}}_{r}\right| = \mathcal{F}_{dr}^{e}$$

Since $\mathcal{F}_{\mathrm{dr}}^{\mathrm{e}}$ remains constant, then $\dot{\mathcal{F}}_{\mathrm{dr}}^{\mathrm{e}} = 0$

Then, (25) becomes

$$0 = r_r(\mathcal{F}_{dr}^{e} - x_M i_{ds}^{e})/x_R$$

Then,

$$\mathcal{F}_{dr}^{e} = x_M i_{ds}^{e} \tag{27}$$

Sub in (17) leads

$$i_{dr}^{e} = 0$$

Equation (24) becomes

$$0 = -r_r\, x_M i_{qs}^{e}/x_R + \omega_s \mathcal{F}_{dr}^{e}/\omega_b$$

Then,

$$\omega_s = \frac{\omega_b r_r i_{qs}^{e}}{x_R i_{ds}^{e}} \tag{28}$$

And,

$$T_e = \frac{3P}{4\omega_b}\frac{x_M^2}{x_R} i_{ds}^{e} i_{qs}^{e} \tag{29}$$

Now, in MTPA strategy, the objective is to maximize T_e while minimizing the stator current i_s^e , which is equal to:

$$|i_s^e| = \sqrt{\left(i_{qs}^{e}\right)^2 + (i_{ds}^{e})^2} \tag{30}$$

The stator current equation draws a circle trajectory in the plane of $i_{ds}^e - i_{qs}^e$, as shown in Figure 3, in which deferent currents draw deferent concentrate circles, while a certain constant torque can draw the green curve. Deferent operation points are extracted from the intersection points between the torque curve and stator current circles.

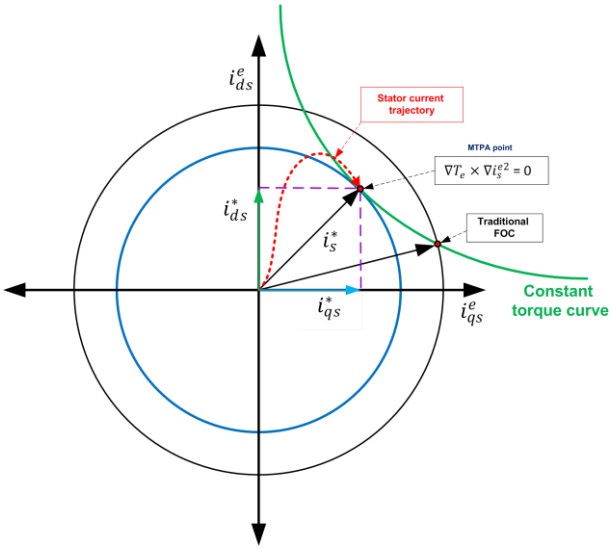

Figure 3. Maximum torque per ampere point.

According to Lagrange's theory, the stator current is minimal when the torque curve is tangential to the current circle. Alternatively, the stator current is minimal when the slopes (gradients) of the two curves are equal [1, 2, and 5].

Or, $\nabla T_e \times \nabla i_s^{e\,2} = 0$

Then, the minimization criteria (α) is the determinant of the cross operation

$$\alpha = \nabla T_e \times \nabla i_s^{e2} = \begin{bmatrix} i & j & k \\ \dfrac{\partial T_e}{\partial i_{ds}^e} & \dfrac{\partial T_e}{\partial i_{qs}^e} & 0 \\ \dfrac{\partial i_s^2}{\partial i_{ds}^e} & \dfrac{\partial i_s^2}{\partial i_{qs}^e} & 0 \end{bmatrix}$$

$$\alpha = \frac{\partial T_e}{\partial i_{ds}^e} \cdot \frac{\partial i_s^2}{\partial i_{qs}^e} - \frac{\partial T_e}{\partial i_{qs}^e} \cdot \frac{\partial i_s^2}{\partial i_{ds}^e} = 0$$

$$\Longrightarrow \alpha = 2({i_{qs}^e}^2 - {i_{ds}^e}^2) = 0$$

$$\Longrightarrow i_{qs}^e = \pm\, i_{ds}^e \tag{31}$$

And $$\theta = tan^{-1} \frac{i_{qs}^e}{i_{ds}^e} = \pi/4$$

According to this context, the maximum torque point that gives minimum stator current can be shown in Figure 3. Substituting (31) in (28) gives the final criteria of the MTPA strategy:

$$\omega_s|_{MTPA} = \frac{\omega_b r_r}{x_R} \tag{32}$$

And, from the torque (29), the desired q-axis current control can be found as:

$$i_{ds}^{e\ *}|_{MTPA} = \sqrt{\frac{4\omega_b}{3P}\frac{x_R}{x_M^2}T_e^{\ est}} \tag{33}$$

Where $T_e^{\ est}$ is the estimated motor's torque.

$$\mathcal{F}_{dr}^{e\ *}|_{MTPA} = x_M i_{ds}^{e\ *}|_{MTPA} = \sqrt{\frac{4\omega_b x_R}{3P}T_e^{\ est}} \tag{34}$$

$$i_{qs}^{e\ *}|_{MTPA} = \frac{4\omega_b}{3P}\frac{x_R}{x_M}\frac{T_e^{\ *}}{\mathcal{F}_{dr}^{e\ *}|_{MTPA}} \tag{35}$$

Where $T_e^{\ *}$ is the desired controlled torque.

Accordingly, if the controlled torque reference equals the estimated torque, then $i_{ds}^{e\ *} = i_{qs}^{e\ *}$ and the MTPA mode operates. The maximum stator current limit for obtaining rated flux and torque can be found from (36) by substituting $i_{qs}^{e\ *}$ and $i_{ds}^{e\ *}$in the MTPA mode,

$$I_s|_{max} = \sqrt{\left(i_{qs}^{e\ *}\right)^2 + (i_{ds}^{e\ *})^2} \tag{36}$$

$$I_s|_{max} = \sqrt{2}\frac{4}{3P}\frac{x_R}{x_M} \tag{37}$$

4. Considering rotor iron losses

Minimizing stator current is very important for reducing stator and rotor winding losses. Unfortunately, this cannot enhance the rotor iron loss. Rotor iron losses in induction motors encompass various types and can significantly impact motor performance. These losses primarily include the stray losses in the rotor core caused by the eddy current and hysteresis loss [7,11]. This leads to heat generation, energy wastage, and reduced efficiency. These losses can be reduced by controlling the magnetizing current by exploiting the MTPA strategy. The rotor iron losses can be represented by equivalent resistor R_w, as shown in Figure 4.

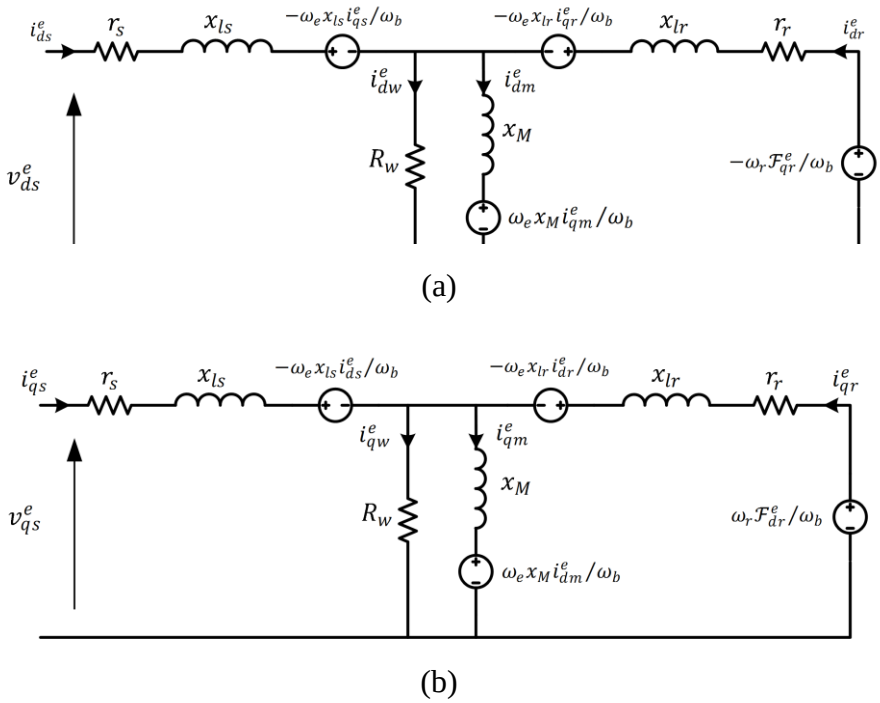

Figure 4. Equivalent circuit considering iron loss, (a) d-axis, (b) q-axis.

The equivalent iron loss current is known as working or watt current ($i^e_{dw} - i^e_{qw}$), which branches from the magnetizing current. According to the machine theory, the voltage across the equivalent iron loss resistance R_w has two parts: electrical- and rotational-induced EMF; then, the dq-axis iron loss currents are [1, 7, and 18]:

$$i^e_{qw} = \frac{\dot{\mathcal{F}}^e_{qm} + \omega_e \mathcal{F}^e_{dm}}{\omega_b R_w} \tag{38}$$

$$i^e_{dw} = \frac{\dot{\mathcal{F}}^e_{dm} - \omega_e \mathcal{F}^e_{qm}}{\omega_b R_w} \tag{39}$$

In motoring action, the electrical EMF is very small, so it can be neglected,

$$i^e_{qw} = \frac{\omega_e \mathcal{F}^e_{dm}}{\omega_b R_w} = \frac{\omega_e x_M i^e_{dm}}{\omega_b R_w} \tag{40}$$

$$i^e_{dw} = \frac{-\omega_e \mathcal{F}^e_{qm}}{\omega_b R_w} = \frac{-\omega_e x_M i^e_{qm}}{\omega_b R_w} \tag{41}$$

The Kirchhoff's current law on the magnetizing node gives

$$i^e_{qm} = i^e_{qs} + i^e_{qr} - i^e_{qw} \tag{42}$$

$$i^e_{dm} = i^e_{ds} + i^e_{dr} - i^e_{dw} \tag{43}$$

Then, (18)–(21) become:

$$i_{qs}^{e} = \frac{\mathcal{F}_{qs}^{e} - x_M(i_{qr}^{e} - i_{qw}^{e})}{x_S} \tag{44}$$

$$i_{ds}^{e} = \frac{\mathcal{F}_{ds}^{e} - x_M(i_{dr}^{e} - i_{dw}^{e})}{x_S} \tag{45}$$

$$i_{qr}^{e} = \frac{\mathcal{F}_{qr}^{e} - x_M(i_{qs}^{e} - i_{qw}^{e})}{x_R} \tag{46}$$

$$i_{dr}^{e} = \frac{\mathcal{F}_{dr}^{e} - x_M(i_{ds}^{e} - i_{dw}^{e})}{x_R} \tag{47}$$

$$v_{qs}^{e} = r_s(\mathcal{F}_{qs}^{e} - x_M(i_{qr}^{e} - i_{qw}^{e}))/x_S + \dot{\mathcal{F}}_{qs}^{e}/\omega_b + \omega_e\mathcal{F}_{ds}^{e}/\omega_b \tag{48}$$

$$v_{ds}^{e} = r_s(\mathcal{F}_{ds}^{e} - x_M(i_{dr}^{e} - i_{dw}^{e}))/x_S + \dot{\mathcal{F}}_{ds}^{e}/\omega_b - \omega_e\mathcal{F}_{qs}^{e}/\omega_b \tag{49}$$

$$0 = r_r(\mathcal{F}_{qr}^{e} - x_M(i_{qs}^{e} - i_{qw}^{e}))/x_R + \dot{\mathcal{F}}_{qr}^{e}/\omega_b + \omega_s\mathcal{F}_{dr}^{e}/\omega_b \tag{50}$$

$$0 = r_r(\mathcal{F}_{dr}^{e} - x_M(i_{ds}^{e} - i_{dw}^{e}))/x_R + \dot{\mathcal{F}}_{dr}^{e}/\omega_b - \omega_s\mathcal{F}_{qr}^{e}/\omega_b \tag{51}$$

For rotor FOC combining with MTPA tracking (see appendix B),

$$\mathcal{F}_{dr}^{e} = \mathcal{F}_{dm}^{e} = x_M(i_{ds}^{e} - i_{dw}^{e})\ ;\ i_{dr}^{e} = 0 \tag{52}$$

$$\omega_s|_{MTPA} = \frac{\omega_b\, r_r\, i_{qm}^{e}}{x_{lr}\, i_{dm}^{e}} \tag{53}$$

$$i_{ds}^{e\ *}\big|_{MTPA} = -i_{dr}^{e} + i_{dm}^{e} + i_{dw}^{e} = i_{dm}^{e} - \frac{\omega_e\, x_M\, i_{qm}^{e}}{\omega_b\, R_w} \tag{54}$$

$$\mathcal{F}_{dr}^{e\ *}\big|_{MTPA} = 2\omega_b \sqrt{\frac{\frac{x_R\, T_e^{est}}{3P}}{1 + \frac{\omega_e\, x_M^2}{x_{lr}\, R_w}}} \tag{55}$$

For more details, see appendix C.

$$i_{qm}^{e} = \frac{4\, x_{lr}\, \omega_b\, T_e^{*}}{3P\, x_M\, \mathcal{F}_{dr}^{e\ *}\big|_{MTPA}} \tag{56}$$

$$i_{qs}^{e\ *}\big|_{MTPA} = \left(1 + \frac{x_M}{x_{lr}}\right) i_{qm}^{e} + \left(1 - \frac{x_M}{x_{lr}}\right) \frac{\omega_e\, x_M}{\omega_b\, R_w}\, i_{dm}^{e} \tag{57}$$

Combining (40), (52) and (54) gives:

$$i_{ds}^{e\ *}\big|_{MTPA} = \frac{\mathcal{F}_{dr}^{e\ *}\big|_{MTPA}}{x_M} - \frac{\omega_e\ x_M\ i_{qm}^e}{\omega_b\ R_w} \tag{58}$$

5. Fractional-order PI controller

The fractional-order proportional-integral (FOPI) controller represents a significant advancement in control system design, particularly for applications requiring precise and robust performance [4]. Unlike traditional PI controllers, which rely on integer-order calculus, FOPI controllers employ fractional calculus, offering additional freedom through adjustable orders of integration. This flexibility allows for a more refined tuning of the controller parameters, leading to improved stability, robustness, and response time performance. The unique characteristics of FOPI controllers make them particularly effective in handling complex, nonlinear, and dynamic systems, providing superior control to conventional methods. These features can be exploited in the PI speed controller [13,20].

Fractional-order calculus is the field that transacts with the ability to power the integral operator by a fractional number. Analytically, the fractional-order calculus can be described in multiple ways. The widespread presentation is the differ-integral fundamental operator, defined by Caputo [21], ${}_{\mathrm{t_o}}^{\mathrm{C}}\mathcal{D}_{\mathrm{t}}^{\beta}$, where t_o and t are the lower and upper boundaries of the operation, β is the fraction order, and C is Caputo's sign. That is defined as:

$${}_{t_o}^{C}\mathcal{D}_t^{\beta} = \begin{cases} \dfrac{d^{\beta}}{dt} & if\ \beta > 0, \\ 1 & if\ \beta = 0, \\ \displaystyle\int_{t_o}^{t} (d\tau)^{-\beta} & if\ \beta < 0. \end{cases} \tag{59}$$

Caputo's definition of fraction derivation can be presented as:

$${}_{t_o}^{C}\mathcal{D}_t^{\beta}\, y(t) = \frac{1}{\Gamma(n-\beta)} \int_{t_o}^{t} \frac{y_{(\tau)}^{n}}{(t-\tau)^{\beta-n+1}}\, d\tau\ ,\ \text{For}\ \ (\mathrm{n}-1 < \beta < n) \tag{60}$$

This carries an essential property: With Caputo's derivation, the initial conditions for fractional-order differentials have identical forms as for integer-order differential equations. One advantage of using this description is offering an easy presentation for initial and limitation conditions, in which the derivative of any constant value equals zero. In the time domain, an n-term of fractional-order differential equations is presented as

$$\begin{aligned} a_k\ \mathcal{D}^{\delta_k}\ y(t) + \ a_{k-1}\ \mathcal{D}^{\delta_{k-1}}\ y(t) + \cdots + a_0\ \mathcal{D}^{\delta_0}\ y(t) \\ = b_m\ \mathcal{D}^{\alpha_m}\ u(t) + \ b_{m-1}\ \mathcal{D}^{\alpha_{m-1}}\ u(t) + \cdots + b_0\ \mathcal{D}^{\alpha_0} u(t) \end{aligned} \tag{61}$$

Where $\mathcal{D}^{\beta} \equiv {}_{0}^{C}\mathcal{D}_t^{\beta}$, δ_k and α_k are real positive numbers, and $\delta_k > \delta_{k-1} > \cdots > \delta_0 > 0$ and $\alpha_k > \alpha_{k-1} > \cdots > \alpha_0 > 0$.

The fractional-order transfer function can be obtained by taking the Laplace transformation of (61):

$$G_k(s) = \frac{Y(s)}{U(s)} = \frac{b_m\ s^{\alpha_m}\ +\ b_{m-1}\ s^{\alpha_{m-1}}\ + \cdots + b_0\ s^{\alpha_0}}{a_k\ s^{\delta_k}\ +\ a_{k-1}\ s^{\delta_{k-1}}\ + \cdots + a_0\ s^{\delta_0}} \tag{62}$$

The PI controller is a versatile closed-loop controlling mechanism widely used in industrial applications. The fractional-order controller (FOC) $PI^{\lambda}D^{\gamma}$ was proposed in [22] as a generalization of the PID controller with integrator of real order λ and differentiator of real order γ. The transfer function of such controller in the Laplace domain has this form:

$$G_{PI^{\lambda}D^{\gamma}}(s) = k_P + \frac{k_I}{s^{\lambda}} + k_D\ s^{\gamma} \tag{63}$$

Where $k_P,\ k_I,\ and\ k_D$ are the proportional, integral, and differential gains, respectively. $\lambda\ and\ \gamma$ are real positive numbers. In reality, a natural controlling system has fractional characteristics in nature. However, the system's fractionality may be very small. Considerably, approximating the integer order of the fractional system causes a significant difference between the natural system and the mathematical model [23]. In spite of this, unfortunately, for simplicity, the integral order form of the PID controller is broadly used in many industrial applications. In this work, the speed controller loop utilizes a PI compensator system. Then, the fractional-order controller is reduced to PI^{λ} controller by setting $\gamma = 0$,

$$G_{PI^{\lambda}}(s) = k_P + \frac{k_I}{s^{\lambda}} \tag{64}$$

In this context, the controller variable is limited to $k_P,\ k_I,$ and λ. There are various methods presented in the literature for evaluating these parameters. Most of these methods depend on the desired dynamic response. Besides, there are many meta-heuristic optimization techniques presented to obtain the optimum parameters. In this work, the optimum controller parameters are evaluated using the particle swarm optimization algorithm (a well-known optimization algorithm). The optimization process aims to minimize a multi-objective fitness function consisting of two parts—the integral time square error, which represents the dynamic and steady-state evaluation, and the stator current value. Minimizing this fitness function leads to enhanced speed performance at minimum stator current. The obtained parameters after 100 iterations are $k_P = 12.5, k_I = 5.7,$ and $\lambda = 0.77$. For more details, refer to [2,22,23].

6. Results and discussion

This section presents the simulation results of the fractional-order field-oriented control based on maximum torque per ampere FOPI-FOC-MTPA techniques, with and without iron loss consideration. This provides critical investigation forms, highlighting the effectiveness of the proposed methods compared with the conventional FOC method presented in [2]. Figure 5 shows the outlines of the overall system's simulation of such conceded iron loss. The induction motor parameters are illustrated in Appendix A.

Figure 6 demonstrates the trajectory contour of the dq-stator current under conventional field-oriented control (FOC), revealing that while the direct current component remains nearly

constant, the quadrature component increases significantly with torque-load increases at two operating points, (TL1) and (TL2). In contrast, Figure 7 illustrates the trajectory contour of the dq-stator current under conventional FOPI-FOC-MTPA, showing that $i_{ds}^{e\,*}$ and $i_{qs}^{e\,*}$ are equal for both loads, indicating improvement in the current values.

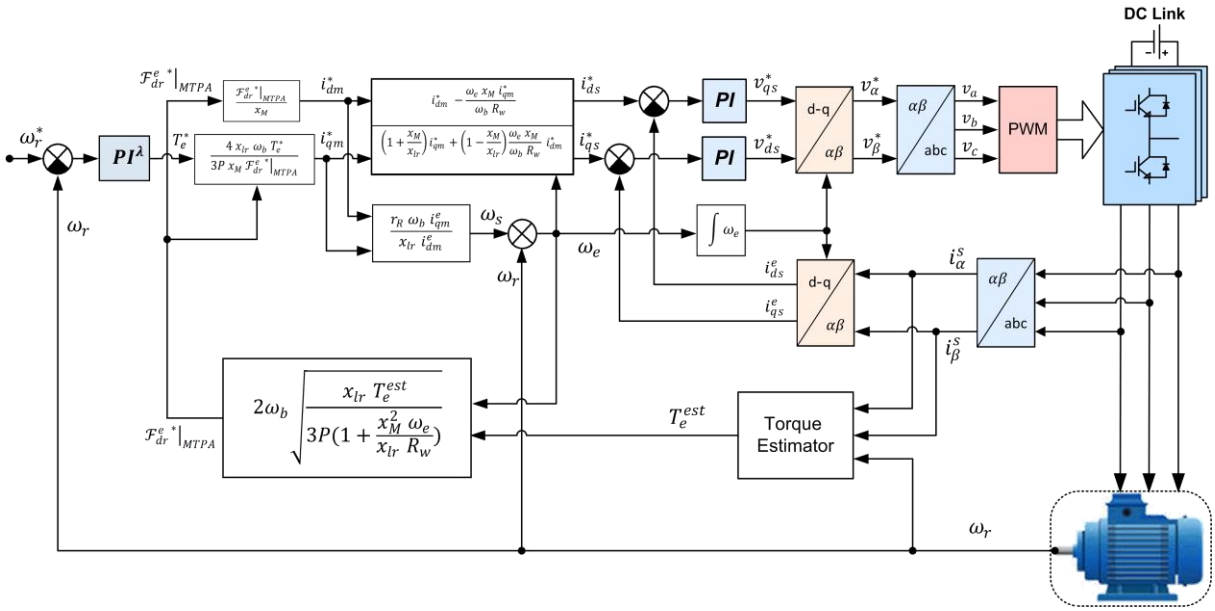

Figure 5. FOPI-FOC-MTPA simulation considering iron loss.

This comparison demonstrates that the proposed strategy's starting current is higher than that of the conventional method. Still, this happens shortly and then significantly reduces to the settled operation current by tracking the maximum torque per ampere point, which can be evaluated by calculating the area under curves. Figure 8 presents the speed, torque, and dq-axis currents of the proposed FOPI-MTPA method, showcasing excellent speed tracking and reduced stator current under full-load operation. That can be shown by the fast rise time, small overshot, acceptable settling time, and low stator current.

Figures 9 and 10 further validate the proposed method's performance in four-quadrant operations. Figure 9 shows the rated speed and torque performances under a step response speed reference. Meanwhile, Figure 10 examines the four-quadrant accelerating and decelerating rated speed and torque performances. Both investigations confirm the robustness of the proposed method under dynamic conditions. Results show excellent and stable full-load operation in motoring, reversing, and regenerative modes, which enable the motor to be used in various applications. Figure 11 compares stator currents between conventional FOC, FOPI-FOC-MTPA, and FOPI-FOC-MTPA with iron loss consideration under full-load conditions. Performances demonstrate the superior performance of the proposed FOPI-FOC-MTPA method, particularly in reducing stator current—it is reduced by about 33% in FOPI-FOC-MTPA-Iron and about 45% in FOPI-FOC-MTPA. Besides, the average starting current is reduced by about 35%–40% compared with the traditional FOC. In this case, it is essential to investigate the rotor speed performance. Figure 12 shows a comparison step response of the three systems. Obviously, the speed performance is somewhat degraded in the proposed methods in terms of rise time and overshoot (increased by about 8% and

0.5%, respectively) and steady-state error (about 0.5%). This can be explained logically by the fact that a high degree of performance requires high consuming power. Since the consumption power is reduced, this will undoubtedly affect the speed performance. It can be said with complete confidence that this change in performance can be overlooked in exchange for the benefits offered by the proposed method of reducing consumed power. The comparison shows that the proposed strategy gives a high degree of acceptability of the motor's performance, which is compatible with the conventional method; this proves that the added modifications did not affect the traditional field-oriented response.

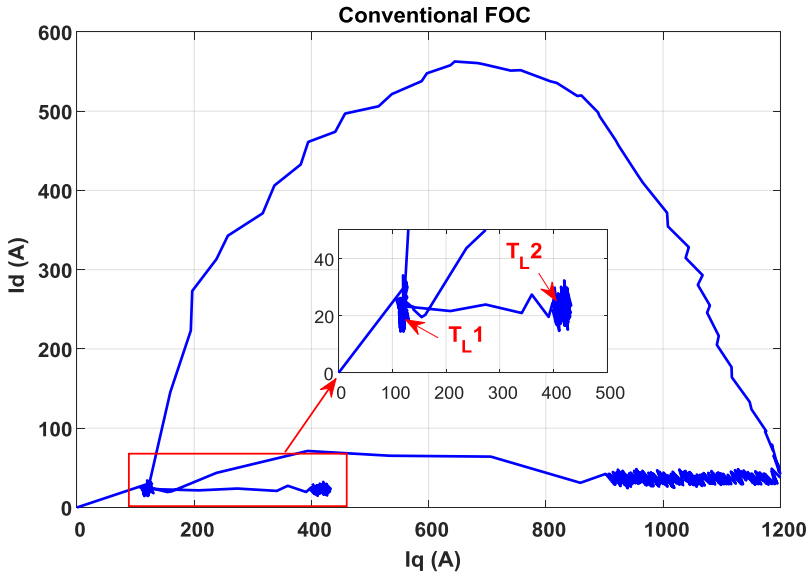

Figure 6. Stator current trajectory of the conventional FOC.

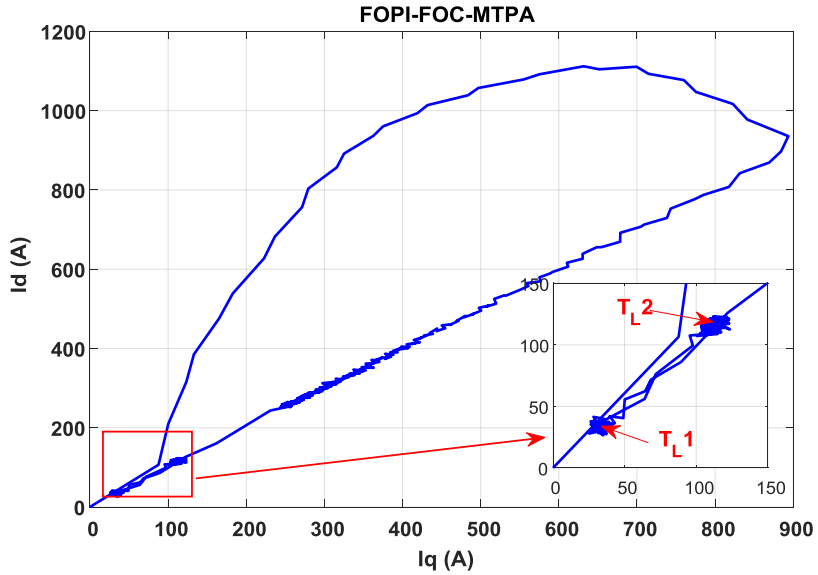

Figure 7. Stator current trajectory of the proposed controller.

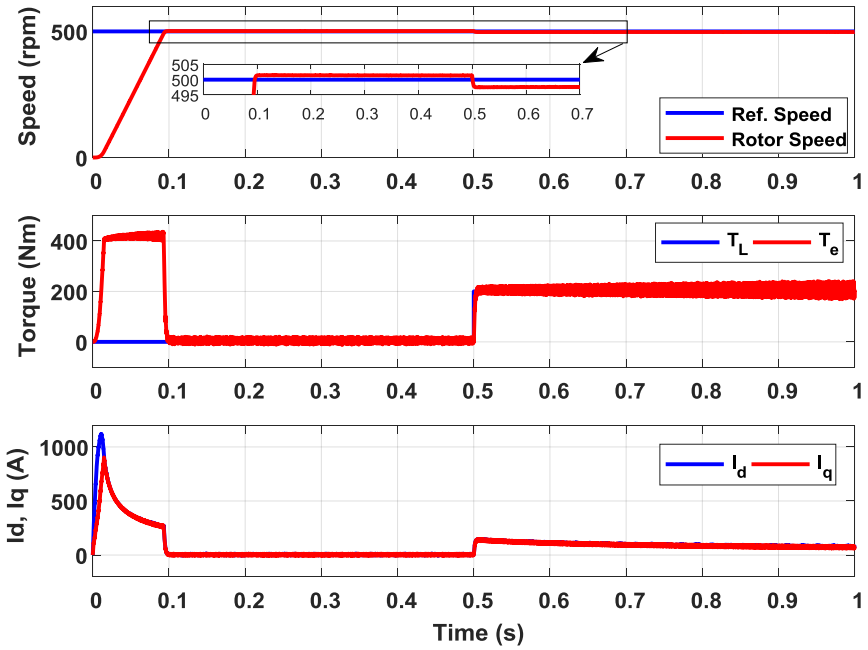

Figure 8. Speed, torque, and dq-axis current.

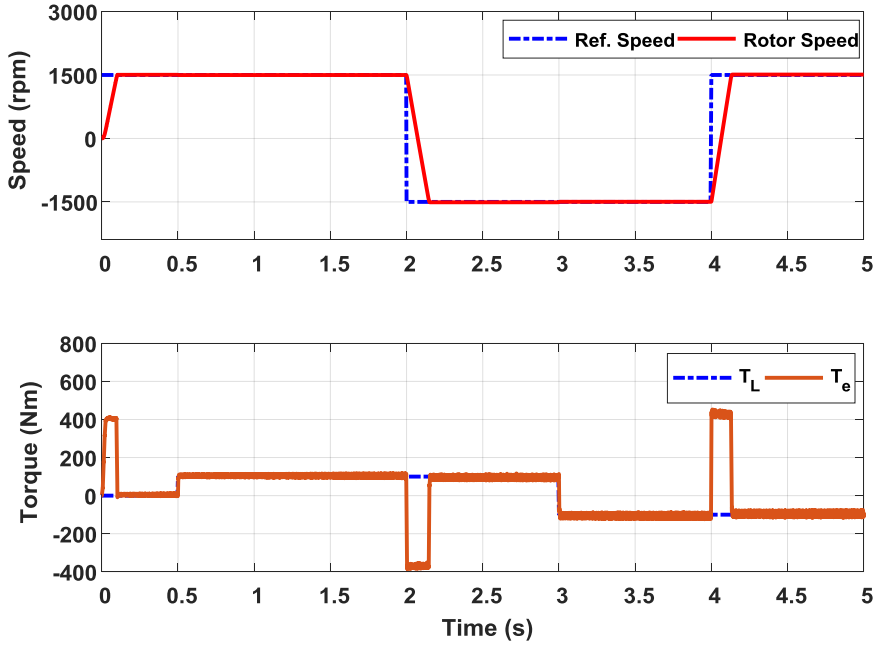

Figure 9. Step response four-quadrant operation.

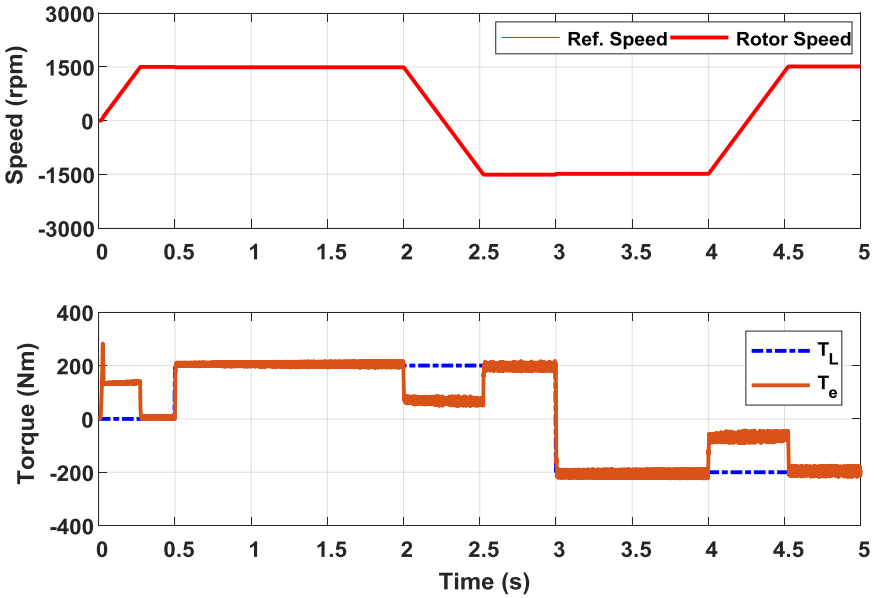

Figure 10. Ramp response four-quadrant operation.

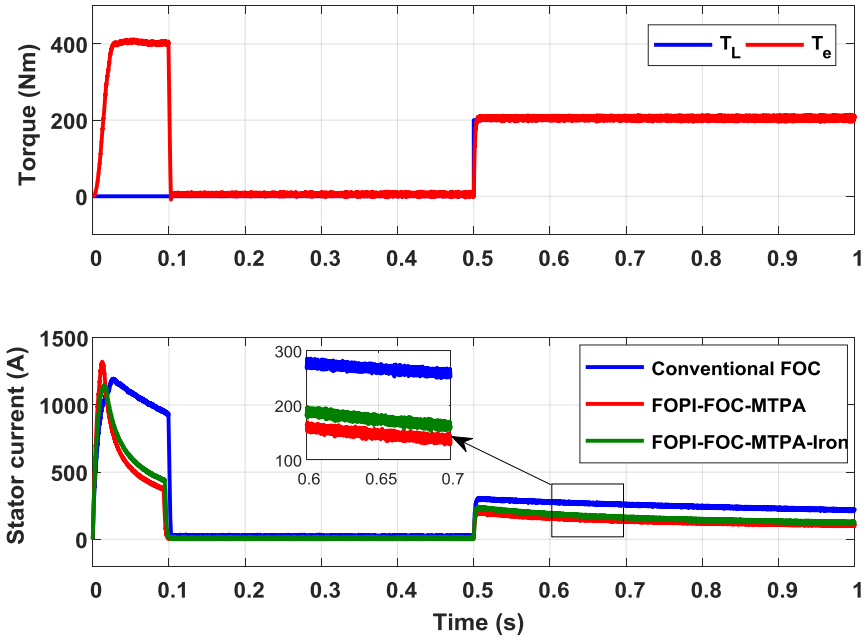

Figure 11. Comparison of stator currents.

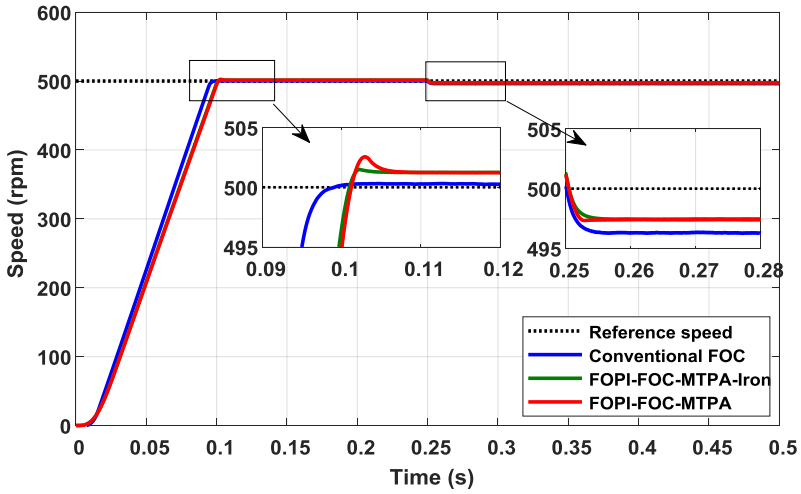

Figure 12. Comparison of speed performances.

The contribution of this work can be clearly illustrated by calculating the torque-to-ampere ratio for different operating conditions. Figure 13 shows the torque per ampere ratio for variable speed commands with constant full load torque; one can see that the ratio is considerably increased by an average of about 24% in FOPI-FOC-MTPA-Iron and about 39% in FOPI-FOC-MTPA. Figure 14 shows the torque per ampere ratio at constant speed and variable load torque. Results show that the ratio in FOPI-FOC-MTPA is higher than the conventional FOC; however, in FOPI-FOC-MTPA-Iron, the ratio may equal that of traditional FOC in low torque and exceed that for high torque values.

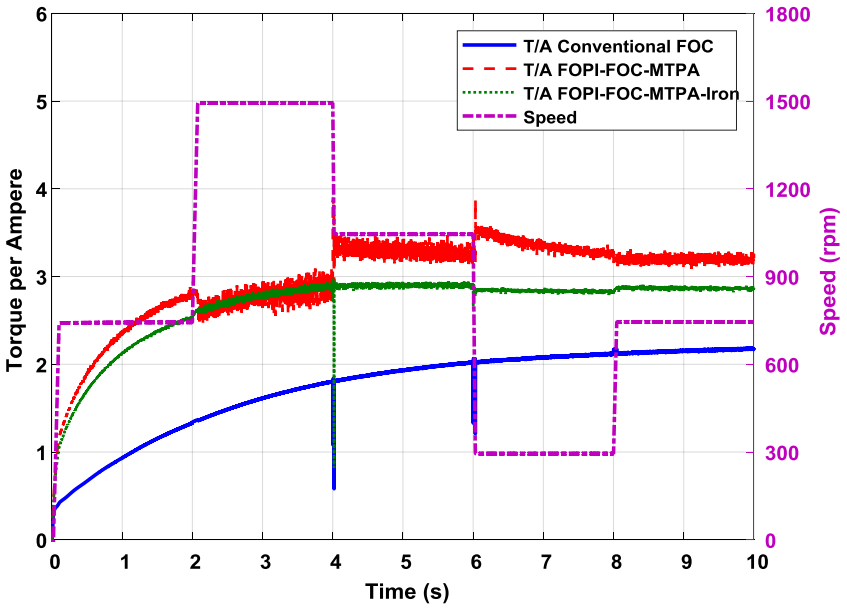

Figure 13. Torque/ampere ratio for constant torque and variable speed.

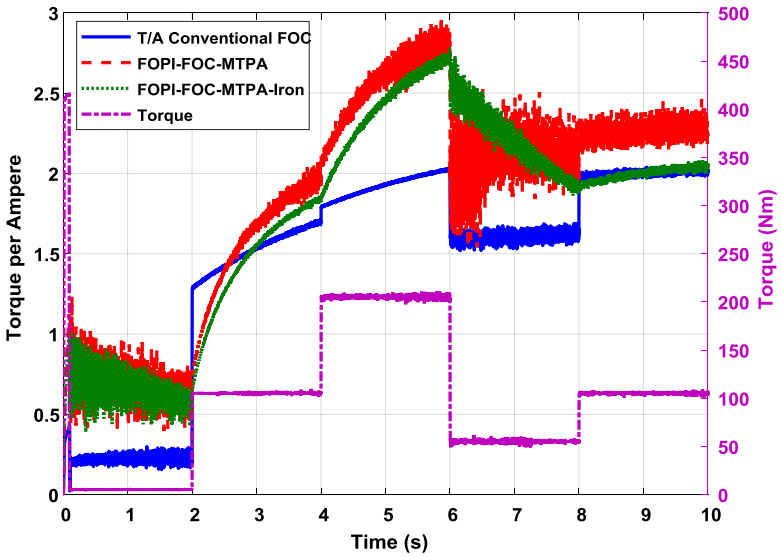

Figure 14. Torque/ampere ratio for constant speed and variable torque.

Furthermore, the contribution of the proposed methods can be verified by calculating the consumed power in kWh. Figure 15 depicts the consumed power for a certain period (1000 s) under full load and variable speed. The consumed kWh decreases by about 12% in FOPI-FOC-MTPA-Iron and about 17% in FOPI-FOC-MTPA.

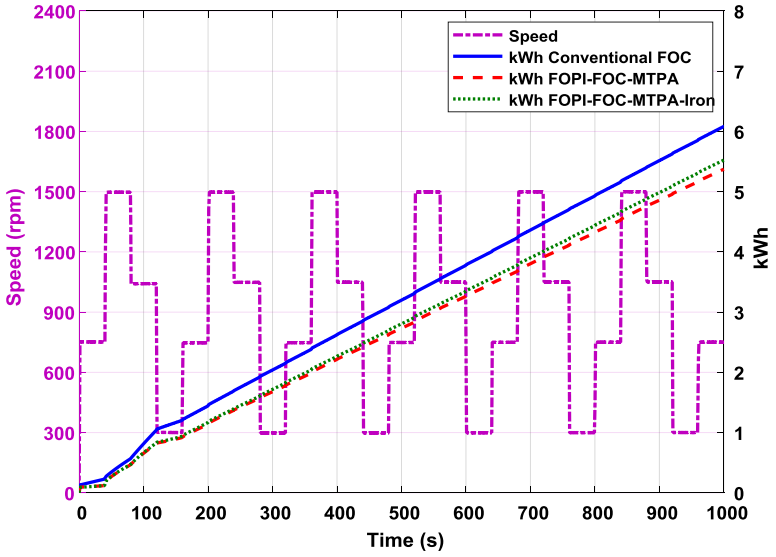

Figure 15. Consumed kWh under constant torque and variable speed conditions.

The results and data collected by the simulations confirm the enhanced performance characteristics, which include a significant reduction in stator current and losses and a notable increase in energy efficiency. These outcomes underscore the effectiveness of the proposed FOPI

control combined with FOC and MTPA strategies. The efficacy and applicability of this method are particularly relevant in the context of advanced motor control systems, where energy efficiency is paramount. The technique is especially suitable for battery-powered applications such as electric vehicles, where optimizing energy consumption highly affects extended battery life, reduced operational costs, and improved overall performance. The results validate that the FOPI-FOC-MTPA method meets the requirements for such high-demand applications, offering a promising solution for the future of electric motor control systems.

7. Conclusions

In this paper, a controlling strategy is presented to optimize the performance of the induction motor. A combination of fractional-order proportional-integral controller and field-oriented control is presented based on the maximum torque per ampere tracking. The method integrates the features of the FOPI controller—enhanced tuning flexibility and robustness—with the benefits of the MTPA strategy, such as improved efficiency and reduced power consumption. The FOPI-FOC-MTPA approach optimizes the produced torque while minimizing stator current, which leads to enhancing motor performance and energy efficiency. The optimum parameters of the FOPI controller are designed using the particle swarm optimization. This method allows for finer tuning of the controller's parameters and more acceptable dynamic behavior than the traditional PI tuning methods. For further efficiency enhancement, the rotor iron loss is incorporated in the analysis (which is closest to reality) to enhance efficiency and reduce consumed current. This improvement was at the expense of speed performance, as the performance deteriorated slightly from that of the traditional method. However, in practice, this is not considered a real deficiency in the motor’s performance compared to the great benefit obtained from reducing the current and power consumed. Results show that the proposed approach significantly exceeds the conventional FOC in terms of drawing current and power consumption, with a 31%–47% and 35%–40% reduction in stator current and average starting current, respectively. Besides, the torque/ampere ratio is increased by about 24%–39%, with a 12%–17% decrease in consumed kWh for a specific period. This work can be extended in future research by practical implementation and experimental validation of the FOPI-FOC-MTPA approach in real-world applications. Also, developing adaptive algorithms could aid in real-time tuning of the controller parameters to adjust dynamic performance. Furthermore, the proposed method's resilience should be assessed regarding parameter variations, external disturbances, and model uncertainties, improving it to meet the evolving demands of modern controller applications.

Author contributions

Fadhil A. Hasan: Methodology, Software, Investigation, Supervision, Validation, Visualization and Writing – review & editing; Lina J. Rashad: Conceptualization, Data curation, Formal Analysis and Writing – original draft. All authors have read and agreed to the published version of the manuscript.

Conflict of interest

The authors declare there is no conflict of interest in this paper.

References

1. Hrkel M, Vittek J and Biel Z (2012) Maximum torque per ampere control strategy of induction motor with iron losses. *2012 ELEKTRO, Rajecke Teplice, Slovakia*, 185–190, https://doi.org/10.1109/ELEKTRO.2012.6225635
2. Hasan F, Abdulrahim T, Lina J (2020) Robust decoupled controller of induction motor by combining PSO and Kharitonov's theorem. *Engineering Science and Technology, an International Journal* 23: 1415–1424. https://doi.org/10.1016/j.jestch.2020.04.004
3. Wasynczuk O, Sudhoff SD, Corzine KA, Tichenor JL, Krause PC, Hansen IG, et al. (1998) A maximum torque per ampere control strategy for induction motor drives. *IEEE T Energy Conver* 13: 163–169, https://doi.org/10.1109/60.678980
4. Kumar DM, Mudaliar HK, Cirrincione M, Mehta U, Pucci M (2018) Design of a Fractional Order PI (FOPI) for the Speed Control of a High-Performance Electrical Drive with an Induction Motor. *2018 21st International Conference on Electrical Machines and Systems (ICEMS)*, 1198–1202. https://doi.org/10.23919/ICEMS.2018.8549407
5. Kousalya V, Singh B (2023) Optimized Reference Points Based Vector Control of Induction Motor Drive for Electric Vehicle. *IEEE T Ind Appl* 59: 4164–4174, https://doi.org/10.1109/TIA.2023.3272534
6. Ding Q, Yang Z, Sun X, Lu C (2023) Accurate Modeling and Optimal Rotor Flux Control of a Bearingless Induction Motor With the Specific Pole. *IEEE T Ind Electron* 71: 5553–5563. https://doi.org/10.1109/TIE.2023.3290248
7. Bašić M, Vukadinović D, Grgić I (2023) Model Predictive Current Control of an Induction Motor Considering Iron Core Losses and Saturation. *Processes* 11: 2917. https://doi.org/10.3390/pr11102917
8. Lažek T, Pazdera I, Toman M (2022) Comparison and Simulation of Two Loss Minimization Algorithms for Field-oriented Control of Induction Motor. *2022 IEEE 20th International Power Electronics and Motion Control Conference (PEMC)*, 216–222. https://doi.org/10.1109/PEMC51159.2022.9962920
9. Kousalya V, Singh B (2022) Optimum Flux Based Vector Control of Induction Motor Drive For Electric Vehicle. *2022 IEEE IAS Global Conference on Emerging Technologies (GlobConET)*, 293–299. https://doi.org/10.1109/GlobConET53749.2022.9872172
10. Accetta A, Cirrincione M, D'Ippolito F, Pucci M, Sferlazza A (2022) Input–Output Feedback Linearization Control of a Linear Induction Motor Taking Into Consideration Its Dynamic End-Effects and Iron Losses. *IEEE T Ind Appl* 58: 3664–3673. https://doi.org/10.1109/TIA.2022.3160409
11. Attaianese C, Monaco MD, Tomasso G (2021) Maximum Torque Per Watt (MTPW) field-oriented control of induction motor. *Electric Eng*, 2611–2623. https://doi.org/10.1007/s00202-021-01238-0
12. Eftekhari SR, Davari SA, Naderi P, Garcia C, Rodriguez J (2019) Robust Loss Minimization for Predictive Direct Torque and Flux Control of an Induction Motor With Electrical Circuit Model. *IEEE T Power Electr* 35: 5417–5426. https://doi.org/10.1109/TPEL.2019.2944190
13. Usman H, Rehman H, Mukhopadhyay S (2018) Electric Vehicle Traction System Performance Enhancement Using FO-PI Controller. *2018 IEEE Vehicle Power and Propulsion Conference (VPPC)*, 1–5. https://doi.org/10.1109/VPPC.2018.8604969

14. Salahmanesh M, Zarchi H, Hesar M (2019) Lyapunov - Based Input-Output Feedback Linearization Control of Induction Motor drives Considering Online MTPA Strategy and Iron Loss. *2019 27th Iranian Conference on Electrical Engineering (ICEE)*, 697–701. https://doi.org/10.1109/IranianCEE.2019.8786507
15. Khurram A, Rehman H, Mukhopadhyay S, Ali D (2018) Comparative Analysis of Integer-order and Fractional-order Proportional Integral Speed Controllers for Induction Motor Drive Systems. *Journal of Power Electronics* 18: 723–735. https://doi.org/10.6113/JPE.2018.18.3.723
16. Madhusudhana G, Srikanth G (2018) Comparative Study of Maximum Torque Control by PI ANN of Induction Motor. *International Journal of Applied Engineering Research* 13: 4620–4625.
17. Mosaddegh Hesar H, Abootorabi Zarchi H, Ayaz Khoshhava M (2019) Online maximum torque per ampere control for induction motor drives considering iron loss using input–output feedback linearization. *IET Electric Power Appl* 13: 2113–2120. https://doi.org/10.1049/iet-epa.2019.0400
18. Bose BK (2002) *Modern Power Electronics and AC Drives*. Prentice Hall, Upper Saddle River, NJ.
19. Krause PC, Wasynczuk O, Sudhoff SD (2013) *Analysis of Electric Machinery and Drive Systems*. Power, Energy and Industry Applications, Wiley & Sons Ltd.
20. Nosheen T, Ali A, Chaudhry MU, Zazarenko D, Shaikh IU, Bolshev V, et al. (2023) A Fractional Order Controller for Sensorless Speed Control of an Induction Motor. *Energies* 16: 1901. https://doi.org/10.3390/en16041901
21. Salih A, Humod T, Hasan F (2019) Optimum Design for PID-ANN Controller for Automatic Voltage Regulator of Synchronous Generator. *2019 4th Scientific International Conference Najaf (SICN)*, 74–79. http://doi:10.1109/SICN47020.2019.9019367
22. Cokmez E, Ati ç S, Peker F, Kaya I (2018) Fractional-order PI Controller Design for Integrating Processes Based on Gain and Phase Margin Specifications. *IFAC-Papers On Line* 51: 751–756. https://doi.org/10.1016/j.ifacol.2018.06.206
23. Salman S, Humod T, Hasan F (2022) Dynamic voltage restorer based on particle swarm optimization algorithm and adaptive neuro-fuzzy inference system. *Bulletin of Electrical Engineering and Informatics* 11: 3217–3227. http://doi:10.11591/eei.v11i6.4023

Appendices

Appendix A

Table 1. Induction motor parameters.

Parameter	Value	Unit
Power	50	Hp
Voltage	460, 3-phase	V
Frequency	50	Hz
Stator resistance	0.087	Ω
Rotor resistance	0.0128	Ω
Stator leakage inductance	0.0001	H
Rotor leakage inductance	0.0008	H
Magnetizing inductance	0.0347	H
No. of poles	4	pole
Moment of inertia	0.662	$Kg.m^2$
Friction factor	0.1	N.m.s

Appendix B

Derivation of (53):
From (50):

$$0 = -r_R x_M (i^e_{qs} - i^e_{qw})/x_R + \omega_s \mathcal{F}^e_{dr}/\omega_b$$

$$\mathcal{F}^e_{dr} = x_M (i^e_{ds} - i^e_{dw})$$

$$r_R (i^e_{qs} - i^e_{qw})/x_R = \omega_s (i^e_{ds} - i^e_{dw})/\omega_b$$

$$\omega_s = \frac{r_R\ \omega_b (i^e_{qs} - i^e_{qw})}{x_R\ (i^e_{ds} - i^e_{dw})} = \frac{r_R\ \omega_b (i^e_{qm} - i^e_{qr})}{i^e_{dm}}$$

$$= \frac{r_R\ \omega_b}{i^e_{dm}} * \left(i^e_{qm} + i^e_{qm}\ \frac{x_M}{x_{lr}} \right), \qquad i^e_{qr} = -i^e_{qm}\ \frac{x_M}{x_{lr}}$$

$$\therefore\ \omega_s = \frac{r_R\ \omega_b\ i^e_{qm}}{x_{lr}\ i^e_{dm}}$$

Appendix C

Derivation of (55):

$$i^e_{qs} = -i^e_{qr} + i^e_{qm} + i^e_{qw}$$

$$\mathcal{F}^e_{qr} = x_{lr}\, i^e_{qr} + x_M (i^e_{qs} - i^e_{qw}) \implies i^e_{qr} = \frac{-x_M}{x_{lr}} (i^e_{qm} - i^e_{qw})$$

$$\therefore\ i_{qs}^{e} = \frac{x_M}{x_{lr}}(i_{qm}^{e} - i_{qw}^{e}) + i_{qm}^{e} + i_{qw}^{e}$$

$$i_{qs}^{e} = (1 + \frac{x_M}{x_{lr}})\ i_{qm}^{e} + (1 - \frac{x_M}{x_{lr}})\ i_{qw}^{e}$$

$$0 = -r_R x_M (i_{qs}^{e} - i_{qw}^{e})/x_R + \omega_s \mathcal{F}_{dr}^{e}/\omega_b$$

$$0 = -r_R((1 + \frac{x_M}{x_{lr}})\ i_{qm}^{e} + (1 - \frac{x_M}{x_{lr}})\ i_{qw}^{e} - i_{qw}^{e})/x_R + \omega_s \mathcal{F}_{dr}^{e}/x_M \omega_b$$

$$i_{qm}^{e}\ \frac{r_R}{x_r}\left(1 + \frac{x_M}{x_{lr}}\right) = \mathcal{F}_{dr}^{e}\ \frac{r_R}{x_r}(\frac{x_M\ \omega_e}{x_{lr}\ \omega_b\ R_w} + \frac{x_r\ \omega_s}{r_r\ x_M\ \omega_b})$$

$$\frac{4\ x_{lr}\ \omega_b T_e^{est}}{3\ P\ \mathcal{F}_{dr}^{e}\ x_M}(x_r) = \mathcal{F}_{dr}^{e}(\frac{x_M\ \omega_e}{x_{lr}\ \omega_b\ R_w} + \frac{1}{x_M\ \omega_b})$$

$$\mathcal{F}_{dr}^{e\ *}\big|_{MTPA} = 2\omega_b \sqrt{\frac{x_{lr}\ T_e^{est}}{3P(1 + \frac{x_M^2\ \omega_e}{x_{lr}\ R_w})}}$$